

Star Formation in the ISO¹ Atlas of Bright Spiral Galaxies

George J. Bendo,^{2,3,4} Robert D. Joseph,^{2,3} Martyn Wells,⁵ Pascal Gallais,⁶ Martin Haas,⁷ Ana M. Heras,^{8,9} Ulrich Klaas,⁷ René J. Laureijs,^{8,9} Kieron Leech,^{9,10} Dietrich Lemke,⁷ Leo Metcalfe,⁹ Michael Rowan-Robinson,¹¹ Bernhard Schulz,^{9,12} and Charles Telesco¹³

ABSTRACT

We investigate star formation along the Hubble sequence using the ISO Atlas of Spiral Galaxies. Using mid-infrared and far-infrared flux densities normalized by K-band flux densities as indicators of recent star formation, we find several trends. First, star formation activity is stronger in late-type (Sc - Scd) spirals than in early-type (Sa - Sab) spirals. This trend is seen both in nuclear and disk activity. These results confirm several previous optical studies of star formation along the Hubble sequence but conflict with the conclusions of most of the previous studies using IRAS data, and we discuss why this might be so. Second, star formation is significantly more extended in later-type spirals than in early-type spirals. We suggest that these trends in star formation are a result of differences in the gas content and its distribution along the Hubble sequence, and it is these differences that promote star formation in late-type spiral galaxies. We also search for trends in nuclear star formation related to the presence of a bar or nuclear activity. The nuclear star formation activity is not significantly different between barred and unbarred galaxies. We do find that star formation activity appears to be inhibited in LINERs and transition objects compared to H II galaxies. The mean star formation rate in the sample is $1.4 M_{\odot} \text{ yr}^{-1}$ based on global far-infrared fluxes. Combining these data with CO data gives a mean gas consumption time of $6.4 \times 10^8 \text{ yr}$, which is ~ 5 times lower than the values found in other studies. Finally, we find excellent support for the Schmidt Law in the correlation between molecular gas masses and recent star formation in this sample of spiral galaxies.

Subject headings: galaxies: evolution — galaxies: spiral — stars: formation

1. Introduction

1.1. Scientific Background

Spiral galaxies have been recognized as sites of ongoing star formation since the definition of the Hubble sequence (Hubble 1926). However the relation between star formation activity and the location on the Hubble sequence has been a continuing controversy for the past twenty years.

Early optical studies comparing star formation activity in spiral galaxies included Stauffer (1982), Kennicutt & Kent (1983), Kennicutt (1983). They found a general trend in star formation activity with Hubble type, with stronger star formation in Sc spirals than in Sa spirals. However, Scoville et al. (1983), using ground-based $10 \mu\text{m}$ observations, demonstrated that star formation activity was not correlated with any global galaxy prop-

91125 USA; bschulz@ipac.caltech.edu

¹³Department of Astronomy, University of Florida, P.O. Box 112055, Gainesville, Florida 32611, USA; telesco@astro.ufl.edu

¹Based on observations with ISO, an ESA project with instruments funded by ESA Member States (especially the PI countries: France, Germany, the Netherlands and the United Kingdom) and with the participation of ISAS and NASA.

²University of Hawaii, Institute for Astronomy, 2680 Woodlawn Drive, Honolulu, HI 96822, USA; bendo@ifa.hawaii.edu, joseph@ifa.hawaii.edu

³Visiting Astronomer at the Infrared Telescope Facility, which is operated by the University of Hawaii under contract from the National Aeronautics and Space Administration.

⁴Visiting Astronomer at the UH 2.2 m Telescope at Mauna Kea Observatory, Institute for Astronomy, University of Hawaii.

⁵UK Astronomy Technology Center, Royal Observatory Edinburgh, Blackford Hill, Edinburgh EH9 3HJ, Scotland, UK; mw@roe.ac.uk

⁶CEA/DSM/DAPNIA Service d'Astrophysique, F-91191 Gif-sur-Yvette, France; gallais@discovery.saclay cea.fr

⁷Max-Planck-Institut für Astronomie, Königstuhl 17, D-69117, Heidelberg, Germany; haas@mpia-hd.mpg.de, klaas@mpia-hd.mpg.de, lemke@mpia-hd.mpg.de

⁸Astrophysics Division, Space Science Department of ESA, ESTEC, P.O. Box 299, 2200 AG Noordwijk, Netherlands; aheras@ests2.estec.esa.nl, rlaureij@rssd.esa.int

⁹ISO Data Center, Astrophysics Division, ESA, Villafranca del Castillo, 28080 Madrid, Spain; lmetcalf@iso.vilspa.esa.es

¹⁰Saïd Business School, Park End Street, Oxford OX1 1HP, England, UK; kieron.leech@saïd-business-school.oxford.ac.uk

¹¹Astrophysics Group, Imperial College, Blackett Laboratory, Prince Consort Road, London SW7 2BZ, England, UK; m.robinson@ic.ac.uk

¹²IPAC, California Institute of Technology 100-22, Pasadena, CA

erty, including Hubble type. This laid the groundwork for a debate on trends in star formation along the Hubble sequence that continues to the present.

With the advent of IRAS, several new studies on this theme were published, including de Jong et al. (1984), Devereux, Becklin, & Scoville (1987), Pompea & Rieke (1989), Devereux & Young (1991), Isobe & Feigelson (1992), Tomita, Tomita, & Saito (1996), and Devereux & Hameed (1997). Most IRAS studies found no trend in star formation along the Hubble sequence, with the exceptions being Devereux, Becklin, & Scoville (1987) and Pompea & Rieke (1989), who found that Sa galaxies are generally weaker sites of star formation than Sc galaxies, and Devereux & Hameed (1997), who found a population of Sa galaxies with relatively enhanced star formation activity. But optical and ultraviolet studies on the problem also continued, with Donas et al. (1987), Deharveng et al. (1994), and Kennicutt, Tamblyn, & Congdon (1994) all finding trends in increasing star formation along the Hubble sequence from Sa to Sc galaxies. To confuse matters further, Young et al. (1996) found trends in $H\alpha$ surface brightness along the Hubble sequence but they argued that the trend did not necessarily reflect a true trend in star formation activity. Infrared spectroscopy of the C II 158 μm line performed with ISO by Leech et al. (1999) also found a trend in increasing star formation from early- to late-type spiral galaxies, but this survey had a small sample of only 19 spiral galaxies.

Clearly, opinion is sharply divided on star formation activity along the Hubble sequence. Some of the reasons for these discrepant results may include the following. 1) Extinction is always a concern in optical or ultraviolet studies, since star formation regions are always dusty. 2) The IRAS sweep-scan technique is not ideal for measuring the flux from faint, extended sources. For faint, extended galaxies the IRAS point source algorithm may mistake the faint outer regions of the galaxy itself for the background and therefore undermeasure the flux. 3) To normalize for galaxy mass, most IRAS studies divide the far-infrared fluxes by B-band fluxes. Since the B-band fluxes represent the fluxes from the youngest, bluest stars in any galaxy, this tends to cancel out any trend in star formation activity in the far-infrared data. 4) The morphological classifications used are sometimes biased towards star formation. In particular, the Revised Shapley Ames (RSA) Catalog (Sandage & Tammann 1987) uses star formation activity in its classification scheme (Sandage & Bedke 1994), so results on star formation trends found by any paper using the RSA classifications may merely reflect the classification criteria.

1.2. The Design of this Study

As a fresh approach to this question, we have completed a new survey of spiral galaxies with the Infrared Space Observatory (ISO) (Kessler et al. 1996) at mid-

infrared and far-infrared wavelengths, supplemented with ground-based JHK photometry. The data are presented in the ISO Atlas of Spiral Galaxies Bendo et al. (2002) (henceforth referred to as Paper 1). This study incorporates several features that address the concerns mentioned above. 1) We minimize uncertainties related to extinction by working strictly with infrared data. 2) The ISO data has several advantages over IRAS data. ISO has improved sensitivity and angular resolution that enables us to distinguish nuclear from disk emission. Furthermore, ISO operates in a point and integrate mode, and the background is measured separately from locations pre-selected from IRAS cirrus maps, so the flux from faint extended galaxies can be measured more accurately (although the flux measurements are still limited by background structure). 3) We normalize mid-infrared and far-infrared fluxes with K-band fluxes, which represent more accurately the total stellar population than B-band fluxes. 4) We use the Third Reference Catalogue of Bright Galaxies (RC3; de Vaucouleurs et al. (1991)) for galaxy classification, since the RC3 classifications are strictly dependent on morphological features such as the bulge to disk ratio and the tightness of the spiral arms (de Vaucouleurs 1959).

We first summarize the sample selection, observations, and data reduction, the details of which can be found in Paper 1. Next, we discuss our diagnostics for studying star formation activity. Then we present our results on trends in star formation along the Hubble sequence, and we compare these results to previous results and discuss the underlying mechanisms for producing the trends. Next, we examine the galaxies for any possible trends in nuclear star formation related to the presence of a bar or nuclear activity. We conclude by calculating quantitative star formation rates and gas consumption times and by comparing these results to those in the literature.

2. Data

2.1. The Sample

The galaxies in this sample are a subset of a complete, magnitude-limited set of galaxies selected from the RSA Catalog. The sample comprised galaxies with Hubble types between S0 and Sd and with magnitudes $B_T = 12$ or brighter; galaxies in the Virgo Cluster were excluded. A randomly selected, subset of these galaxies was observed by ISO based on target visibility. This produced a total of 77 galaxies that are representative of the range of Hubble types in the RSA Catalog. Additional information on the sample and its properties is presented in Paper 1.

2.2. Observations and Data Analysis

Detailed information on the observations, the data processing, and the measurements themselves are pre-

sented in Paper 1. In short, the 60, 100, and 180 μm photometry was obtained with ISOPHOT (Lemke et al. 1996) and processed with PIA 8.0 (Gabriel et al. 1997), with additional processing to correct for PSF effects. The 12 μm images were taken with ISOCAM (Cesarsky et al. 1996) using the LW10 filter, which covered the range 8-15 μm and were processed with CIA 3.0 (Ott et al. 1997), followed by full processing with CIR, an implementation of the algorithms of Starck et al. (1999) realized by P. Chaniel. The K-band photometric images were mostly taken with QUIRC at the UH 2.2 m telescope, with additional data from NSFCAM and SPEX at the NASA IRTF.

2.3. Star Formation Diagnostics

We seek a diagnostic of recent star formation activity. Both the mid- and far-infrared fluxes represent radiation from dust grains heated by the total stellar radiation field comprised of the diffuse interstellar radiation field (ISRF) which is dominated by the old stellar population, and radiation from recent star formation activity. The 12 μm data includes both PAH spectral line emission and very small grain continuum emission, both heated by the radiation field. While the PAH features will remain relatively unchanging in intensity (or decrease slightly) as the radiation field increases, the continuum does increase, as demonstrated by Dale et al. (2001). The 12 μm data thus includes contributions from both the old stellar population, through the diffuse ISRF, and dust heated by recent star formation. Furthermore, with the exception of some Sd and Sm galaxies, the mid-infrared and far-infrared fluxes are tightly correlated among the galaxies in the sample, as shown in Figure 1. In particular, the mean ratios of the mid-infrared flux to the far-infrared flux in Sa, Sb, and Sc galaxies are statistically identical, as shown in Table 1. This correlation demonstrates that mid-infrared fluxes are as effective as the far-infrared fluxes in tracing the total stellar radiation field.

On the other hand, the K-band flux largely traces the old stellar population, whose thermal emission peaks at $\sim 1.6 \mu\text{m}$. Normalizing the 12 μm flux densities by the flux densities at K therefore largely cancels out the contribution from the old stellar population to the radiation field, so that the 12 μm /K-band flux density ratio is a good diagnostic of recent star formation activity. Similarly, the far-infrared flux densities contain contributions from dust heated by both the diffuse ISRF and from recent star formation activity. Dividing the far-infrared flux densities by the K-band flux densities tends to cancel the contribution from the diffuse ISRF, thus making far-infrared/K flux density ratios a second diagnostic for recent star formation activity. Therefore, we use the mid- and far-infrared fluxes normalized by the K-band fluxes as star formation indicators.

To verify that these indicators are useful, we compare

these flux ratios generated from the Starburst99 model (Leitherer et al. 1999). We ran two test cases with the Starburst99 model: an instantaneous burst of star formation that forms a fixed mass of stars, and a continuous burst of star formation that forms stars at a fixed rate. For each case, we used a Salpeter initial mass function with a slope of -2.35, an upper mass cutoff of $100 M_{\odot}$, and solar metallicities. The other inputs that we used for the model match the defaults for Starburst99. We examine the diagnostic $M_{Bol} - M_K$, effectively the total bolometric flux divided by the K-band flux, which behaves like our normalized mid- and far-infrared fluxes. For comparison, we also examine $M_{Bol} - M_B$, or bolometric fluxes divided by B-band fluxes. This is akin to the far-infrared fluxes normalized with B-band fluxes that are often used in studies that examine trends in star formation along the Hubble sequence.

In Figure 2 we plot $M_{Bol} - M_K$ and $M_{Bol} - M_B$ for the time range between 10^6 and 10^8 yr for an instantaneous burst of star formation, and in Figure 3 the same data are plotted for the continuous star formation model. The colors on the left side of the graphs represent younger stellar populations, while the colors on the right side of the graphs represent older stellar populations. In both plots, the most notable feature is the dip in the $M_{Bol} - M_K$ indicator at 10^7 yr due to the evolution of the most massive stars into the red supergiants that dominate the total K-band emission at that time. It is evident that, for both scenarios, the difference between recent star formation and an evolved stellar population for $M_{Bol} - M_K$ are 1.5 - 2.5 magnitudes, and the K-band normalization provides one magnitude increased discrimination compared to normalization by B-band fluxes. Since the mid- and far-infrared fluxes are proportional to the bolometric luminosity, diagnostics using these fluxes divided by K-band fluxes are useful for tracing recent star formation, and are certainly preferable to diagnostics using B-band fluxes. Real galaxies will of course contain star formation regions lying within populations of older stars, and star formation activity may occur in a series of instantaneous bursts, or be continuous but time-varying. What this exercise does show is that the diagnostics we have chosen are effective for discriminating recent star formation activity.

3. Star Formation Along the Hubble Sequence

3.1. Star Formation Activity

We will examine trends in star formation along the Hubble sequence in three regions of these galaxies. The global regions were defined as the regions within the inner 135 arcsec because it matched the aperture of ISOPHOT observations at 60 and 100 μm . The nuclear regions were defined as the inner 15 arcsec, which corresponds to a diameter in an integer number of pixels that is wider than three times the full width half-maximum of the point

spread function in the ISOCAM images. The disk regions were defined as outside the nuclear regions but within the global regions. To study the global star formation, we use the far-infrared fluxes (the 40 - 220 μm fluxes from Paper 1) normalized by the K-band fluxes for 63 galaxies where we measured both fluxes within 135 arcsec. To study the nuclear and disk star formation, we use the mid-infrared (8-15 μm) fluxes normalized by the K-band fluxes. Nuclear star formation was investigated in 70 galaxies in which fluxes were detected within 15 arcsec at $\geq 3 \sigma$ levels, and disk star formation was explored in 55 galaxies in which fluxes within 135 arcsec were detected at $\geq 3 \sigma$. The use of fixed angular apertures means that the physical areas sampled in each galaxy will vary with the distance to the galaxy. However, the flux ratios used here are uncorrelated with distance, so differences in the physical area sampled should not significantly affect the analysis.

Figures 4 - 6 show histograms of the star formation indicators for each Hubble type. A clear trend can be seen in these histograms, with star formation activity increasing from early-type to late-type galaxies. This trend is seen separately in global, nuclear, and disk star formation, although it is not as well defined in the nuclear regions as it is in the disk regions.

Table 2 presents Gaussian statistics that compare the star formation indicators of each Hubble type. Clearly these statistics show quantitatively a large difference in the star formation activity between Sa - Sab and Sc - Scd galaxies. The difference between mean values of the star formation diagnostics for Sa - Sab and Sc - Scd galaxies is greater than 3σ for all regions, and the difference is nearly 6σ for the disk regions. Because the data may not necessarily obey Gaussian statistics, we also used non-parametric statistical methods to compare Sa - Sab, Sb - Sbc, and Sc - Scd galaxies. Table 3 contains results from applying the Kolmogorov-Smirnov (K-S) test to the diagnostics for two different morphological subsets. The probabilities reported indicate the likelihood that the two populations come from the same distribution (*i.e.* they have similar values). The K-S tests show at the 98 % confidence level that the Sa - Sab and Sc - Scd nuclear star formation diagnostics have distinct values and at better than the 99 % confidence level that the Sa - Sab and Sc - Scd global and disk star formation diagnostics have distinct values.

It has been suggested that use of RSA Catalog classifications for studies such as these can produce spurious correlations, since star formation is included in the classification scheme. The analysis above has used RC3 classifications, but we have repeated the analysis using RSA classifications. We found no changes in the trends or their statistical significance for nuclear or global star formation, but the correlation of disk activity with morphological type went from $\sim 6 \sigma$ to $\sim 8 \sigma$. Evidently the star formation features do make a measurable difference

in the RSA classifications.

These data all clearly show that star formation activity increases along the Hubble sequence from early- to late-type galaxies, with a strong distinction between the star formation activity of Sa - Sab and Sc - Scd galaxies. The trend is clear for the global, nuclear, and disk regions, although it is not as well defined in the nuclear regions.

3.2. Spatial Extent of Star Formation

In Paper 1 we noted that late-type galaxies usually contained well defined star formation structures in their disks while early-type galaxies often did not. Furthermore, some late-type galaxies hosted their strongest sites of star formation in their disks, whereas all early-type galaxies produced their strongest mid-infrared emission from within or near their nuclei. Our qualitative conclusion was that star formation is more centralized in early-type galaxies and more extended in late-type galaxies.

We now attempt to show this trend quantitatively using the 12 μm mid-infrared fluxes. To indicate the central concentration of the star formation activity, we calculate the logarithm of the flux within 15 arcsec divided by the flux within 135 arcsec, or $\log \left(\frac{F_{MIR(15'')}}{F_{MIR(135'')}} \right)$. This quantity will be larger for a centrally concentrated galaxy and smaller for a more extended galaxy. (Taking the logarithm of this quantity is appropriate because we are looking for multiplicative differences in the ratio, which will appear linear in logarithm space.) We perform this analysis for only for those galaxies where the 12 μm flux within the 135 arcsec aperture was detected at the 3σ level. Because this quantity may also be related to the angular width of the galaxy examined, we only use galaxies with similar angular sizes, those with $\log(D_{25})$ values (from RC3) between 1.5 and 1.9. These constraints pared the sample down to 44 galaxies.

Table 4 presents Gaussian statistics on the $\log \left(\frac{F_{MIR(15'')}}{F_{MIR(135'')}} \right)$ values, and Figure 7 presents histograms showing the distribution of values for each Hubble type. Since this data is surely non-Gaussian, we also present probabilities resulting from the K-S test in Table 5. These data show a continuous trend from Sa to Scd with a 5σ significance. Alternatively, the K-S test shows at the 99% level that the Sa-Sab and the Sc-Scd galaxies differ in the spatial extent of their mid-infrared fluxes.

3.3. Discussion

Perhaps ironically, the ISO Atlas results are consistent with nearly all previous optical and ultraviolet studies - including Stauffer (1982), Kennicutt & Kent (1983), Kennicutt (1983), Donas et al. (1987), Kennicutt, Tamblyn, & Congdon (1994), and Deharveng et al. (1994) - but inconsistent with nearly all the earlier infrared pho-

tometric studies. It is intriguing that our infrared approach has confirmed the trends with Hubble type found in optical studies. Does this mean that the issues of extinction mentioned in the Introduction are actually irrelevant? We suggest that extinction is an issue, and the infrared approach provides a statistically stronger conclusion. Unfortunately, it is not possible to make quantitative comparisons because none of the optical studies that reported a trend with Hubble type offered any quantitative assessment of confidence. Most simply showed the global trend graphically as we have done in Figures 4 - 6.

The far-infrared spectroscopic results from Leech et al. (1999) are consistent with the ISO Atlas results, but the only two far-infrared photometric studies with results consistent with these are Devereux, Becklin, & Scoville (1987) and Pompea & Rieke (1989). Both these studies used RSA morphological classifications, and as we have argued above, trends found in samples classified with the RSA Catalog will at least partly reflect the classification criteria rather than true physical trends. The remaining photometric infrared studies, including Scoville et al. (1983), de Jong et al. (1984), Devereux & Young (1991), Isobe & Feigelson (1992), Tomita, Tomita, & Saito (1996), and Devereux & Hameed (1997) found no significant correlation between star formation activity and Hubble type. We suggest that the advantages the ISO measurements provide, both the angular resolution and the point-and-integrate observing mode, compared to IRAS, and the normalization by K-band fluxes rather than by B-band fluxes, are responsible for the different conclusions reached in this study compared to most of the previous infrared studies.

These trends in star formation must reflect physical differences between early- and late-type spiral galaxies. These physical differences can be interpreted in the context of the results from Kennicutt (1989), which states that star formation is related to gas density by a simple power law and that the gas density must exceed a threshold density before star formation is triggered. This must mean that the gas density is more likely to exceed the critical threshold in late-type spiral galaxies than in early-type spirals. In fact, the molecular and total gas surface density does increase from early- to late-type galaxies (Young & Knezek 1989), (Roberts & Haynes 1994), and the ratio of total gas mass to dynamical mass also increases from early- to late-type galaxies (Young & Scoville 1991). This demonstrates that a typical Sc galaxy is more likely than an Sa galaxy to have gas densities high enough to trigger gravitational collapse and star formation. Interestingly, Young et al. (1995) also demonstrate that molecular gas is distributed over a larger area in late-type spiral galaxies than in early-type spiral galaxies. This suggests that our observations of more spatially extended star formation in late-type galaxies compared to early-type galaxies may be the result of the spatial

distribution of molecular gas in spiral galaxies.

4. Dependence of Star Formation on Other Factors

4.1. Relation of Nuclear Star Formation to Bars

4.1.1. Background

Unlike research on variation in star formation along the Hubble sequence, research on how bars may enhance star formation is reaching a consensus, but the paradigm is more complicated than for star formation along the Hubble sequence.

Very early studies on barred galaxies, such as Sérsic & Pastoriza (1965) and Sérsic & Pastoriza (1967), demonstrated that barred galaxies are more likely to host enhanced nuclear star formation. Studies using IRAS data, including de Jong et al. (1984) and Hawarden et al. (1986), demonstrated that barred galaxies have enhanced star formation compared to unbarred galaxies. These results have been confirmed by Devereux (1987), Huang et al. (1996), Ho, Filippenko, & Sargent (1997a), and Roussel et al. (2001), who find the enhancement only in early-type spiral galaxies. These results are not confirmed by Isobe & Feigelson (1992), but their study did not subdivide the data into early- and late-type spiral galaxies, so they may not have been able to find the effect seen by others.

Although these studies tend to agree, most of them rely on IRAS data to detect nuclear enhancements in star formation, even though the IRAS detectors may not adequately isolate nuclear infrared emission from disk emission. Because the data in the ISO Atlas has several advantages in studying star formation, described earlier, we attempt to examine the issue of whether bars enhance star formation. Unfortunately, this sample contains very few early-type galaxies, where the effect is expected to be seen, so we cannot expect to produce a definitive conclusion on this subject.

4.1.2. Analysis

In this analysis, we compare SA, SAB, and SB galaxies for three subsets of galaxies in the sample: Sa - Sab galaxies, Sb - Sbc galaxies, and Sc - Scd galaxies. Since bars specifically affect nuclear star formation, we use the nuclear star formation indicator $\log(\frac{F_{MLR}}{F_K})$. Table 6 presents Gaussian statistics on the $\log(\frac{F_{MLR}}{F_K})$ values. We also present probabilities from applying the K-S test in Table 7.

The Gaussian statistics show very little statistical difference between the SA, SAB, and SB galaxies for any subset. For Sa - Sab galaxies, we have very few galaxies for making a comparison, so more data would be needed to properly determine the presence or absence of a trend. For Sb - Sbc and Sc - Scd galaxies, the number of galax-

ies in the comparison is large enough that the statistics can be treated as meaningful. No difference is found between the SA and SB types for Sb - Sbc galaxies. The data do show an increase in star formation from SA to SB galaxies for Sc - Scd galaxies, but the trend is a statistically weak 2σ trend. The application of the K-S test to the data for all galaxy subsets confirms that there is no significant statistical difference between SA and SB galaxies.

4.1.3. Discussion

The current paradigm suggests that only in some barred galaxies will enhanced star formation be found, and then only in early-type spiral galaxies. The ISO Atlas sample contains too few SA and SAB early-type spiral galaxies to make any definitive statements on how bars may affect nuclear star formation. Some late-type spiral galaxies apparently host enhanced star formation, but the trend is statistically weak, so we cannot make any definitive statements. Clearly, a larger sample of galaxies is required to make stronger statements on the effects of bars. We can however express agreement with most other recent results that demonstrate little enhancement of nuclear star formation in barred late-type galaxies.

4.2. Relation of Nuclear Star Formation Activity to AGN Activity

4.2.1. Background

The association of starbursts with active galactic nuclei (AGNs) has been postulated for both Seyferts and low ionization nuclear emission regions (LINERs). The issues for these two classes of galaxies are different, however.

For Seyferts, the issue is how enhanced star formation activity is connected to the AGN activity. A few studies, such as Rodriguez Espinosa, Rudy, & Jones (1987), Dultzin-Hacyan, Moles, & Masegosa (1988), Heckman et al. (1989), Gonzalez-Delgado & Perez (1993), Colina et al. (1997), González Delgado et al. (1998), and Oliva et al. (1999) have found links between the Seyfert activity and star formation activity, although most suggest that the enhancement in star formation is seen only in Seyfert 2 galaxies. Since the ISO Atlas has superior spatial resolution at mid-infrared wavelengths compared to most other previous infrared studies of the Seyfert/starburst connection, we should be able to examine whether enhanced star formation activity is found in Seyferts. Unfortunately, using the Ho, Filippenko, & Sargent (1997b) classifications for AGN, the sample contains only three Seyfert galaxies.

For LINERs, the issue is whether or not LINER optical line emission is correlated with starburst activity. Three types of excitation mechanisms have been proposed for LINER emission: photoionization from a clus-

ter of hot young stars (Terlevich & Melnick 1985; Shields 1992), photoionization from a power-law source such as an AGN (Ho, Filippenko, & Sargent 1993), and shock excitation (Heckman 1980). It is not clear that only one excitation mechanism is responsible for producing all observed LINER activity, as recent studies have suggested that the LINER class of galaxies may consist of galaxies with different central engines (Larkin et al. 1998) (Alonso-Herrero et al. 2000). If LINER emission is powered by photoionization by hot young stars from a starburst, the nuclei should produce relatively strong mid-infrared emission. If LINER emission is powered by other mechanisms, however, the LINER nuclei may not necessarily be sources of strong mid-infrared emission.

To address these issues, we compare the nuclear star formation activity in Seyferts, LINERs, H II galaxies, and transition objects in our sample that have also been surveyed by Ho, Filippenko, & Sargent (1997b), who classified the galaxies' nuclear activity based strictly on optical spectral line ratios. (NGC 6503 is classified as both a transition object and a Seyfert, but we treat it as a transition object, which is, according to Ho, Filippenko, & Sargent (1997b), the more probable designation for the nuclear activity.) By using this one source of AGN classification, we ensure that the classifications are consistent among the galaxies in the comparison.

4.2.2. Analysis

We compare the various classes of galaxies using the nuclear star formation indicator $\log(\frac{F_{MLR}}{F_K})$, where the fluxes are measured for the inner 15 arcsec. Table 8 presents Gaussian statistics on the $\log(\frac{F_{MLR}}{F_K})$ values, and Figure 8 presents histograms showing the distribution of values for each Hubble type. We also present probabilities from applying the K-S test in Table 9.

It is very apparent from the data that the Seyferts and H II galaxies are sites of stronger mid-infrared activity than the LINERs and transition objects. The LINERs and transition objects also seem to be very similar to each other in terms of nuclear mid-infrared activity, which may indicate that similar physical processes are responsible for the generation of the spectral line emission in both these classes of galaxies. The Gaussian statistics show that the H II galaxies and Seyferts have higher $\log(\frac{F_{MLR}}{F_K})$ values than the LINERs and transition objects. The statistical difference between the H II galaxies and the LINERs and transition objects is $\sim 6\sigma$. The results from the K-S test show that the H II galaxies have a distinctly different distribution of values than the LINERs or transition objects at the 99% confidence level.

4.2.3. Discussion

These results demonstrate very conclusively that the LINERs and transition objects in this sample are, at the very least, not classic starburst galaxies. They could be

either quiescent AGN, or galaxies with shock-dominated nuclear regions. The contrast in mid-infrared emission between the more active Seyferts and the quiescent LINERs is also very striking, although the number of Seyferts in this sample is small. The data may imply that the presence of either circumnuclear material or circumnuclear star formation will boost the AGN activity from the more quiescent LINER level to the more active Seyfert level. However, more work is needed to investigate the connection, specifically a more careful study of the circumnuclear regions of Seyferts and LINERs as well as a mid-infrared survey of all Seyferts and LINERs from the sample in Ho, Filippenko, & Sargent (1997b).

It is noteworthy, but perhaps not surprising, that the H II galaxies and Seyferts are indistinguishable using these photometric diagnostics. This is, after all, the underlying cause of the "starbursts-monsters" controversy (Heckman et al. 1983).

5. Star Formation Rates and Molecular Gas Content

5.1. Global Star Formation Rates

To measure the range of star formation activity in the ISO Atlas sample, we have converted the far-infrared fluxes into quantitative star formation rates by assuming that all the far-infrared flux comes from star formation regions. We use the formula

$$SFR(M_{\odot}yr^{-1}) = 1.76 \times 10^{-10} L_{FIR}(L_{\odot}) \quad (1)$$

where L_{FIR} is the 8 - 1000 μm flux (Kennicutt 1998b). Both Sauvage & Thuan (1992) and Kennicutt (1998a) have emphasized that direct conversion of far-infrared fluxes to star formation rates relies on the assumptions that far-infrared fluxes are emitted from dust heated by star formation regions and that the dust is optically thick. Dust heated by an interstellar radiation field generated by old stars will also produce far-infrared emission, leading to star formation rates that are calculated to be higher than they really are. Nonetheless, we will use this conversion factor as an estimate of the global star formation rates in these galaxies.

First we converted the global 40 - 220 μm fluxes (*i.e.* the fluxes from within the inner 135 arcsec) to 8 - 1000 μm fluxes using the conversion factor 1.192 ± 0.235 . Following a method similar to the one described in Stickel et al. (2000), this conversion factor and its uncertainties were calculated by assuming that the emission in the 8 - 1000 μm range is dominated by a single blackbody component with temperatures ranging between 20 - 40 K and emissivities with wavelength dependence ranging from λ^0 to λ^{-2} . Then luminosities were calculated, and the above formula was applied to convert the luminosities into star formation rates. Figure 9 shows the range of star formation rates. The average star formation

rate is $1.4 M_{\odot} yr^{-1}$, with a maximum of $8.5 M_{\odot} yr^{-1}$ and a minimum of $0.0035 M_{\odot} yr^{-1}$. These results are affected by Malmquist bias because the sample was magnitude-limited. Also, the validity of the conversion factor has not been tested through observations. Nonetheless, these star formation rates are consistent with the spiral disk star formation rates listed in Kennicutt (1998a).

5.2. Gas Consumption Times

Since we have estimated global star formation rates for these galaxies we should also examine whether the galaxies contain sufficient gas to maintain this level of star formation activity over a Hubble time. This issue has been investigated previously by Larson, Tinsley, & Caldwell (1980), Kennicutt (1983), Sandage (1986), Donas et al. (1987), Kennicutt, Tamblyn, & Congdon (1994), and Devereux & Hameed (1997). All of these studies have found gas consumption times of a few times 10^9 yr, which is shorter than a Hubble time. They usually suggest that gas recycling is responsible for increasing the gas consumption time, although only Kennicutt, Tamblyn, & Congdon (1994) have modeled this effect. However, most of the above studies have relied on optical or ultraviolet data for determining star formation rates. Dust extinction in these wavebands may lead to calculated star formation rates that are artificially low, which then may lead to calculated gas consumption times that are artificially high. We attempt to address this issue with our far-infrared data, despite the concerns about using the data to calculate star formation rates mentioned above.

To calculate gas consumption times, we will use the "Roberts time"

$$\tau_R = \frac{M_{gas}}{SFR} \quad (2)$$

suggested by Kennicutt, Tamblyn, & Congdon (1994). For gas masses, we used the CO data from the FCRAO Extragalactic CO Survey (Young et al. 1995) to estimate the gas masses within 135 arcsec apertures. We calculate gas consumption times for the 20 galaxies in the ISO sample for which the CO intensities were detected at the 3σ level in the central beam. The average gas consumption time we calculate is 6×10^8 yr, with a maximum of 1.3×10^9 yr and a minimum of 3×10^8 yr. These gas consumption times seem to be independent of Hubble type or the star formation metrics we used above.

The gas consumption times we calculate are short compared to the few times 10^9 yr values found in most other studies. It is possible that the high star formation rates we calculate are more accurate than those calculated using data from optical and ultraviolet wavebands because of dust extinction issues. Alternatively, our star formation rates could plausibly be high for several reasons. There may be contributions to the far-infrared flux from dust heated by the old stellar population that could

increase our calculated star formation rates. Also, if we had used a different conversion factor to convert infrared flux to star formation, for example that given by Scoville & Young (1983), we would have found gas consumption times on the order of 10^9 yr, which would be more in line with most previous results (most closely with Devereux & Hameed (1997), who also calculated gas consumption times from far-infrared data). However, our global star formation rates are comparable to those listed in Kennicutt’s review (Kennicutt 1998a), so our star formation rates may be correct. In summary, multiple factors may be responsible for the slightly low gas consumption times we find compared to most previous results, but because of uncertainties in the assumptions, we cannot argue that our results are more accurate than most previous calculations.

5.3. Testing the Schmidt law

In discussing the trend in star formation with Hubble type, we suggested that it resulted from the difference in molecular gas content between early- and late-type galaxies. If so, for galaxies where we have both infrared and CO data, we should be able to find the power law relation between star formation and gas density discussed by Schmidt (1959) and Kennicutt (1989). We investigate this with the molecular gas mass data from Young et al. (1995) and do the comparison with star formation activity for global, nuclear, and disk regions separately. For the global analysis we use the star formation rates found above, and for the nuclear and disk analysis we use the 12 and 60 μm flux densities, which have spatial resolutions that are equivalent to or better than the CO data. Because we were limited by the resolution of the CO data, we used 45 arcsec apertures to represent the nuclear regions (instead of the 15 arcsec apertures used in the analysis of star formation trends).

Figure 10 shows the gas masses versus star formation rates normalized by the square of the distance to the galaxies. We use this normalization because both quantities are effectively derived from luminosities; otherwise there may be a spurious correlation since one is effectively plotting D^2 vs. D^2 . The figure shows that the two quantities are very well correlated and can be represented by a simple power law.

Figures 11 and 12 show the normalized gas masses versus 12 and 60 μm flux densities for the nuclear regions of the galaxies. Most of the galaxies lie very nicely along this trend. The exceptions are NGC 1569 (the outlier near the upper left of the figures) and NGC 5236 (the outlier near the upper right of the figures). NGC 1569 is a nearby dwarf galaxy with strong star formation activity, so it may not necessarily follow the same trend as most spiral galaxies.

Figures 13 and 14 show the normalized gas masses versus 12 and 60 μm flux densities for the disk regions

between the 45 and 135 arcsec diameters of galaxies. The trends are not as well defined as for the nuclear regions, particularly at 12 μm . The scatter, particularly at low gas masses, may represent the failure of gas densities to exceed the threshold necessary for star formation as discussed by Kennicutt (1989).

In summary, these comparisons demonstrate an excellent Schmidt law relating molecular gas and either star formation rates or far-infrared flux densities. The trend is seen globally as well as in separate nuclear and disk regions, with occasional deviations from the trend found in unusual objects or in objects where gas masses fail to exceed the threshold for star formation in their disks.

6. Summary

Using the ISO Atlas data for an optically-selected, magnitude-limited sample of spiral galaxies, combined with normalization by K-band flux densities, we have examined the evidence for star formation in three regions of these galaxies: integrated over the entire 135 arcsec of the galaxies (global), the central 15 arcsec (nuclear), and in the disk itself excluding the nuclear region. We have found strong trends in star formation activity along the Hubble sequence in all three regions with statistical significance of $\sim 3\text{-}6\sigma$. We also show that the distribution of star formation regions is more spatially-extended in late-type galaxies than early-type galaxies.

These results confirm most previous optical and ultraviolet investigations of star formation along the Hubble sequence, but do not confirm the findings of an equally large number of such studies using infrared (mostly IRAS) data, which have found no correlations with Hubble type. We suggest that the superior angular resolution in the ISO Atlas data, combined with use of K-band flux densities for normalization, has resolved this long-standing discrepancy between optical and infrared studies.

We argue that the differences in star formation activity along the Hubble sequence may be understood primarily in terms of the differences in the molecular gas density and distribution. We confirm that star formation is well-correlated with molecular gas mass. We suggest that the strength of the star formation activity increases as the gas density increases along the Hubble sequence. Similarly, we suggest that the spatial extent of star formation activity increases as the spatial extent of the molecular gas increases.

We found no enhancement of nuclear star formation in barred galaxies compared to unbarred galaxies, in contrast with many previous results. This may be because the effect is seen chiefly in early-type galaxies and we have few early-type SA and SAB galaxies in the sample. We do find that star formation seems to be inhibited in LINERs and transition objects compared to H II galaxies, suggesting that LINER emission is not powered by

recent starburst activity (at least in nearby galaxies).

From the far-infrared fluxes we estimate star formation rates of $1.4 M_{\odot} \text{ yr}^{-1}$, which is in agreement with previous studies of similar spiral galaxy samples. However, we find gas consumption times of $6 \times 10^{-8} \text{ yr}$, which is about a factor of 5 lower than most previous studies. We do find excellent correlation between molecular gas densities and recent star formation activity in accord with the Schmidt Law.

The ISOPHOT data presented in this paper were reduced using PIA, which is a joint development by the ESA Astrophysics Division and the ISOPHOT Consortium led by MPIA, with the collaboration of the Infrared Processing and Analysis Center (IPAC). Contributing ISOPHOT Consortium institutes are DIAS, RAL, AIP, MPIK, and MPIA.

The ISOCAM data presented in this paper were analysed using ‘CIA’, a joint development by the ESA Astrophysics Division and the ISOCAM Consortium. The ISOCAM Consortium is led by the ISOCAM PI, C. Cesarsky.

This research has been supported by NASA grants NAG 5-3370 and JPL 961566.

REFERENCES

- Alonso-Herrero, A., Rieke, M. J., Rieke, G. H., & Shields, J. C. 2000, *ApJ*, 530, 688
- Bendo, G. J., et al. 2002, *AJ*, 123, 3067
- Cesarsky, C.J., et al. 1996, *A&A*, 315, L32
- Colina, L., Vargas, M. L. G., Gonzalez Delgado, R. M., Mas-Hesse, J. M., Perez, E., Alberdi, A., & Krabbe, A. 1997, *ApJ*, 488, L71
- Dale, D. A., Helou, G., Contursi, A., Silbermann, N. A., & Kolhatkar, S. 2001, *ApJ*, 549, 215
- de Jong, T., Clegg, P. E., Soifer, B. T., Rowan-Robinson, M., Habing, H. J., Houck, J. R., & Aumann, H. H. 1984, *ApJ*, 278, 67
- de Vaucouleurs, G. 1959, *Handbuch der Physik*, 53, 275
- de Vaucouleurs, G., de Vaucouleurs, A., Corwin, H. G., Buta, R. J., Paturel, G., & Fouque, P. 1991, *Third Reference Catalogue of Bright Galaxies* (Berlin: Springer-Verlag)
- Deharveng, J.-M., Sasseen, T. P., Buat, V., Bowyer, S., Lampton, M., & Wu, X. 1994, *A&A*, 289, 715
- Devereux, N. 1987, *ApJ*, 323, 91
- Devereux, N. A., Becklin, E. E., & Scoville, N. 1987, *ApJ*, 312, 529
- Devereux, N. A., & Hameed, S. 1997, *AJ*, 113, 599
- Devereux, N. A., & Young, J. S. 1991, *ApJ*, 371, 515
- Donas, J., Deharveng, J. M., Laget, M., Milliard, B., & Huguenin, D. 1987, *A&A*, 180, 12
- Dultzin-Hacyan, D., Moles, M., & Masegosa, J. 1988, *A&A*, 206, 95
- Gabriel, C., et al. 1997, in *ASP Conf. Ser. 125, Astronomical Data Analysis Software and Systems (ADASS) VI*, ed. G. Hunt & H.E.Payne, (San Francisco: ASP), 108
- González Delgado, R. M., Heckman, T., Leitherer, C., Meurer, G., Krolik, J., Wilson, A. S., Kinney, A., & Koratkar, A. 1998, *ApJ*, 505, 174
- Gonzalez-Delgado, R. M., & Perez, E. 1993, *Ap&SS*, 205, 127
- Hawarden, T. G., Mountain, C. M., Leggett, S. K., & Puxley, P. J. 1986, *MNRAS*, 221, 41P
- Heckman, T. M. 1980, *A&A*, 87, 152
- Heckman, T. M., van Breugel, W., Miley, G. K., & Butcher, H. R. 1983, *AJ*, 88, 1077
- Heckman, T. M., Blitz, L., Wilson, A. S., Armus, L., & Miley, G. K. 1989, *ApJ*, 342, 735
- Ho, L. C., Filippenko, A. V., & Sargent, W. L. W. 1993, *ApJ*, 417, 63
- Ho, L. C., Filippenko, A. V., & Sargent, W. L. W. 1997, *ApJ*, 487, 591
- Ho, L. C., Filippenko, A. V., & Sargent, W. L. W. 1997, *ApJS*, 112, 315
- Huang, J. H., Gu, Q. S., Su, H. J., Hawarden, T. G., Liao, X. H., & Wu, G. X. 1996, *A&A*, 313, 13
- Hubble, E. 1926, *ApJ*, 64, 321
- Isobe, T., and Feigelson, E. D. 1992, *ApJS*, 79, 197
- Kennicutt, R. C. 1983, *ApJ*, 272, 54
- Kennicutt, R. C. 1989, *ApJ*, 344, 685
- Kennicutt, R. C. 1998a, *ARA&A*, 36, 189
- Kennicutt, R. C. 1998b, *ApJ*, 498, 541
- Kennicutt, R. C., & Kent, S. M. 1983, *AJ*, 88, 1094
- Kennicutt, R. C., Tamblyn, P., & Congdon, C. W. 1994, *ApJ*, 435, 22
- Kessler, M.F., et al. 1996, *A&A*, 315, L27
- Larkin, J. E., Armus, L., Knop, R. A., Soifer, B. T., & Matthews, K. 1998, *ApJS*, 114, 59
- Larson, R. B., Tinsley, B. M., & Caldwell, C. N. 1980, *ApJ*, 237, 692
- Leech, K. J., et al. 1999, *MNRAS*, 310, 317
- Leitherer, C., et al. 1999, *ApJS*, 123, 3
- Lemke, D., et al. 1996, *A&A*, 315, L64
- Oliva, E., Origlia, L., Maiolino, R., & Moorwood, A. F. M. 1999, *A&A*, 350, 9
- Ott, S., et al. 1997, in *ASP Conf. Ser. 125, Astronomical Data Analysis Software and Systems (ADASS) VI*, ed. G. Hunt & H.E.Payne, (San Francisco: ASP), 34
- Pompea, S. M., & Rieke, G. H. 1989, *ApJ*, 342, 250
- Roberts, M. S., & Haynes, M. P. 1994, *ARA&A*, 32, 115
- Rodriguez Espinosa, J. M., Rudy, R. J., & Jones, B. 1987, *ApJ*, 312, 555
- Roussel, H., et al. 2001, *A&A*, 372, 406
- Sandage, A. 1986, *A&A*, 161, 89

- Sandage, A., & Bedke, J. 1994, *The Carnegie Atlas of Galaxies*, (Washington: Carnegie Institution)
- Sandage, A., & Tammann, G. A. 1987, *A Revised Shapley-Ames Catalog of Bright Galaxies* 2nd ed. (Washington: Carnegie Institution)
- Sauvage, M., & Thuan, T. X. 1992, *ApJ*, 396, L69
- Schmidt, M. 1959, *ApJ*, 129, 243
- Scoville, N. Z., Becklin, E. E., Young, J. S., & Capps, R. W. 1983, *ApJ*, 271, 512
- Scoville, N., & Young, J. S. 1983, *ApJ*, 265, 148
- Sérsic, J. L., & Pastoriza, M. 1965 *PASP*, 77, 287
- Sérsic, J. L., & Pastoriza, M. 1967 *PASP*, 79, 152
- Shields, J. C. 1992, *ApJ*, 399, L27
- Starck, J. L., et al. 1999, *A&AS*, 134, 135
- Stauffer, J. R. 1982, *ApJS*, 50, 517
- Stickel, M., et al. 2000, *A&A*, 359, 865
- Terlevich, R., & Melnick, J. 1985, *MNRAS*, 213, 841
- Tomita, A., Tomita, Y., & Saito, M. 1996, *PASJ*, 48, 285
- Young, J. S., Allen, L., Kenney, J. D. P., Lesser, A., & Rownd, B. 1996, *AJ*, 112, 1903
- Young, J. S., & Knezek, P. M. 1989, *ApJ*, 347, L55
- Young, J. S., & Scoville, N. Z. 1991, *ARA&A*, 29, 581
- Young, J. S., et al. 1995, *ApJS*, 98, 219

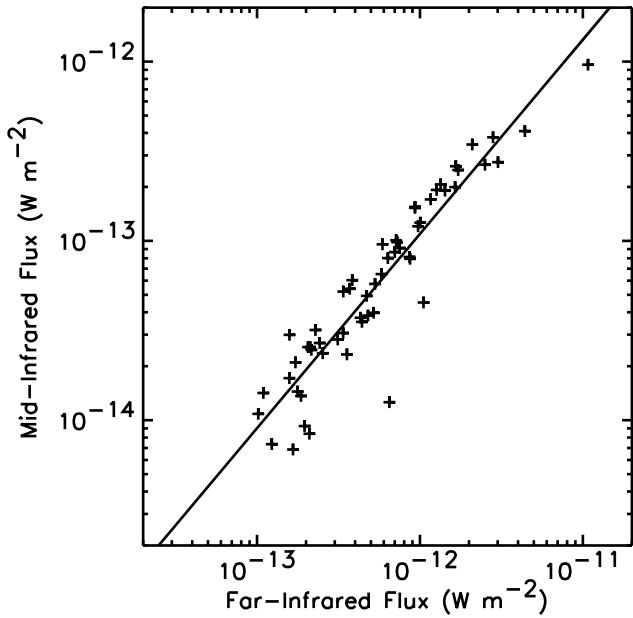


Fig. 1.— Plot of the mid-infrared fluxes within $135''$ versus the far-infrared fluxes within $135''$ for all galaxies detected in both wavebands. The line shows the best fitting power law.

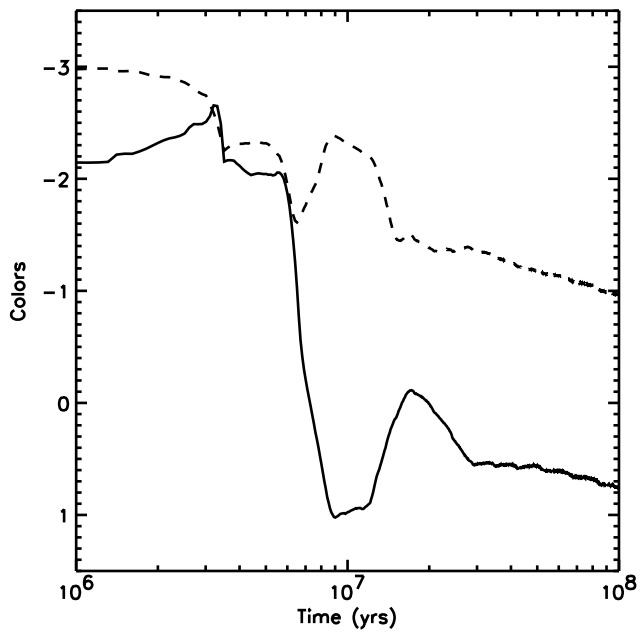


Fig. 2.— Plots of two star formation indicators following an instantaneous burst of star formation, as modeled by Starburst99. The solid line represents $M_{Bol} - M_K$ and the dashed line represents $M_{Bol} - M_B$.

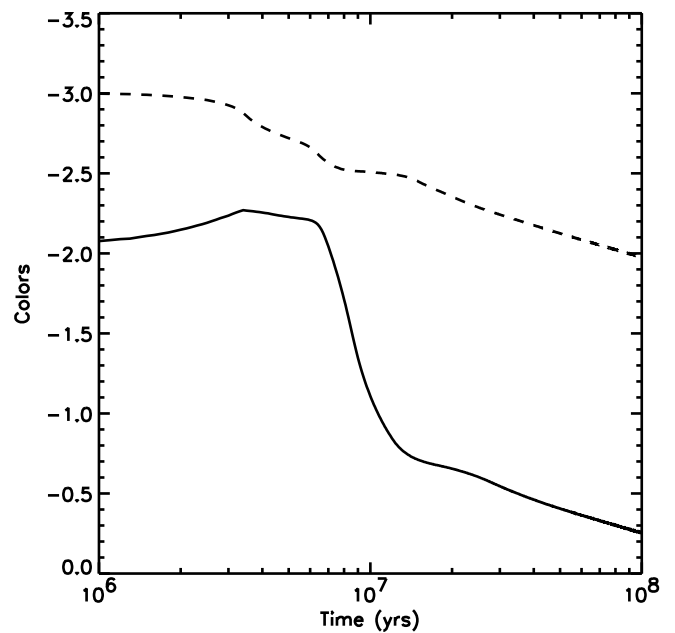


Fig. 3.— Plots of two star formation indicators following the onset of continuous star formation, as modeled by Starburst99. The solid line represents $M_{Bol} - M_K$ and the dashed line represents $M_{Bol} - M_B$.

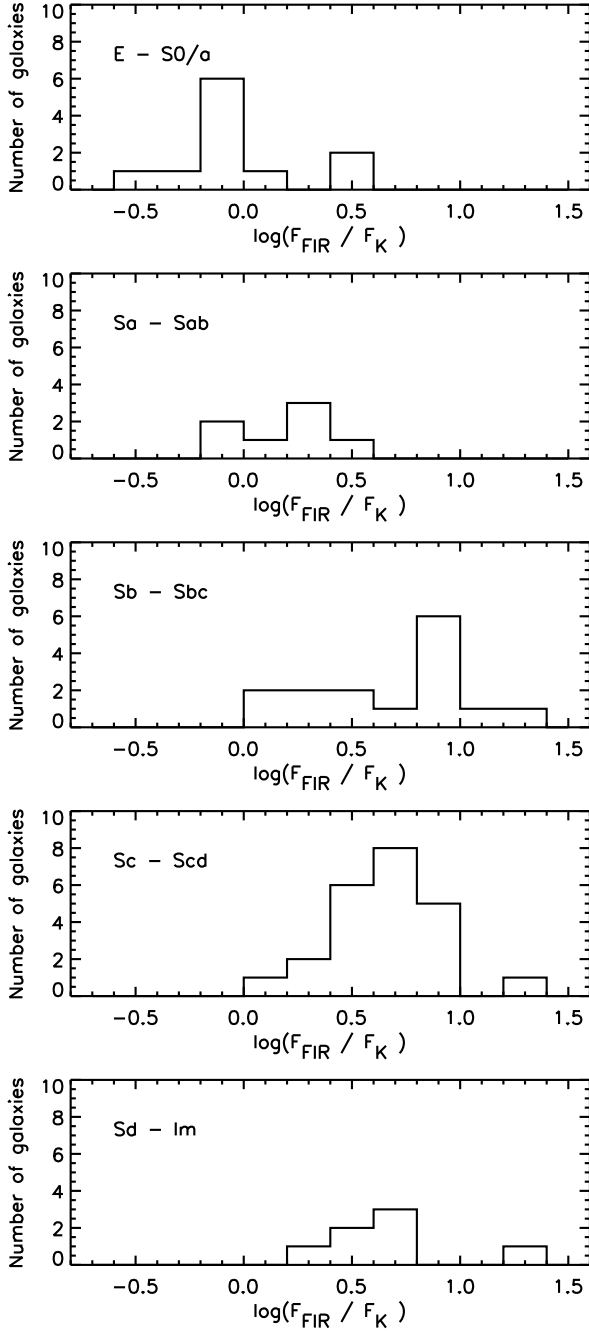


Fig. 4.— Histograms of the global star formation diagnostic $\log(\frac{F_{\text{FIR}}}{F_K})$ for subsets of the galaxies in the sample binned according to Hubble type.

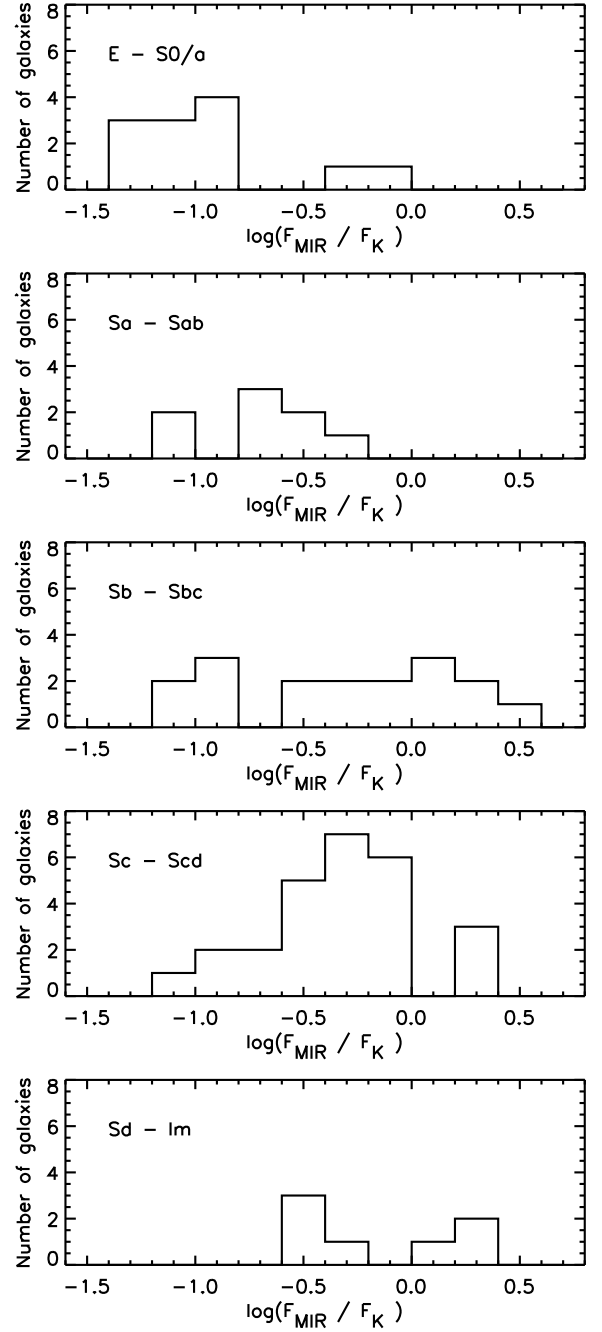


Fig. 5.— Histograms of the nuclear star formation diagnostic $\log(\frac{F_{\text{MIR}}}{F_K})$ for subsets of the galaxies in the sample binned according to Hubble type.

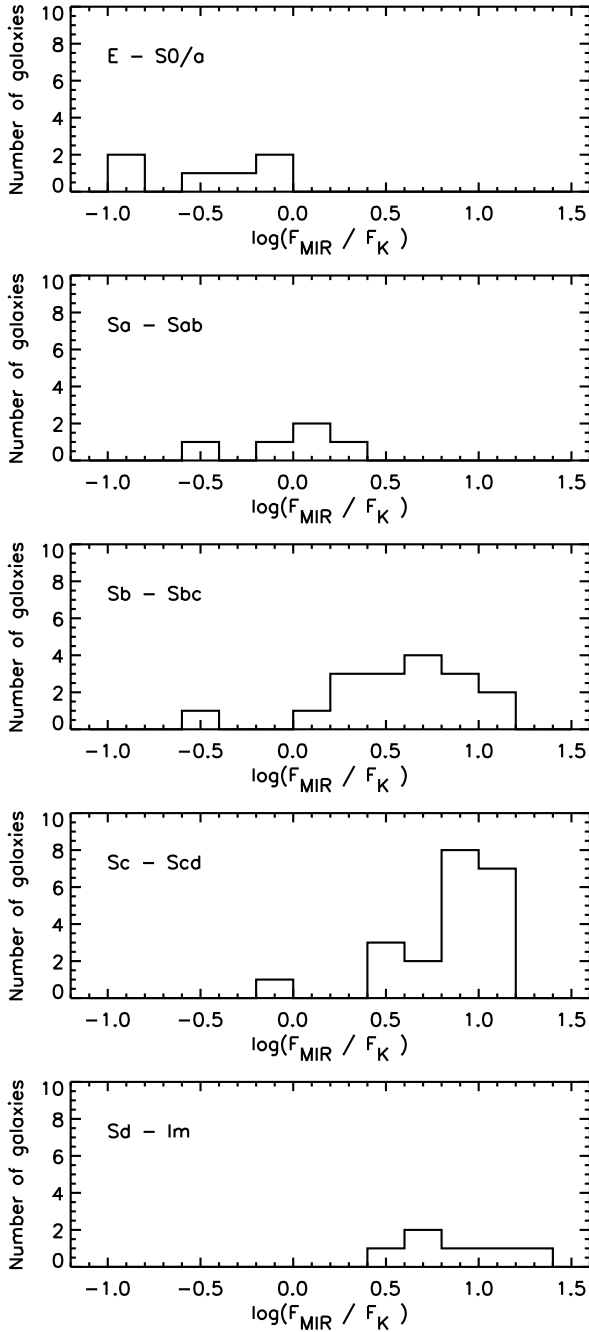


Fig. 6.— Histograms of the disk star formation diagnostic $\log(\frac{F_{MIR}}{F_K})$ for subsets of the galaxies in the sample binned according to Hubble type.

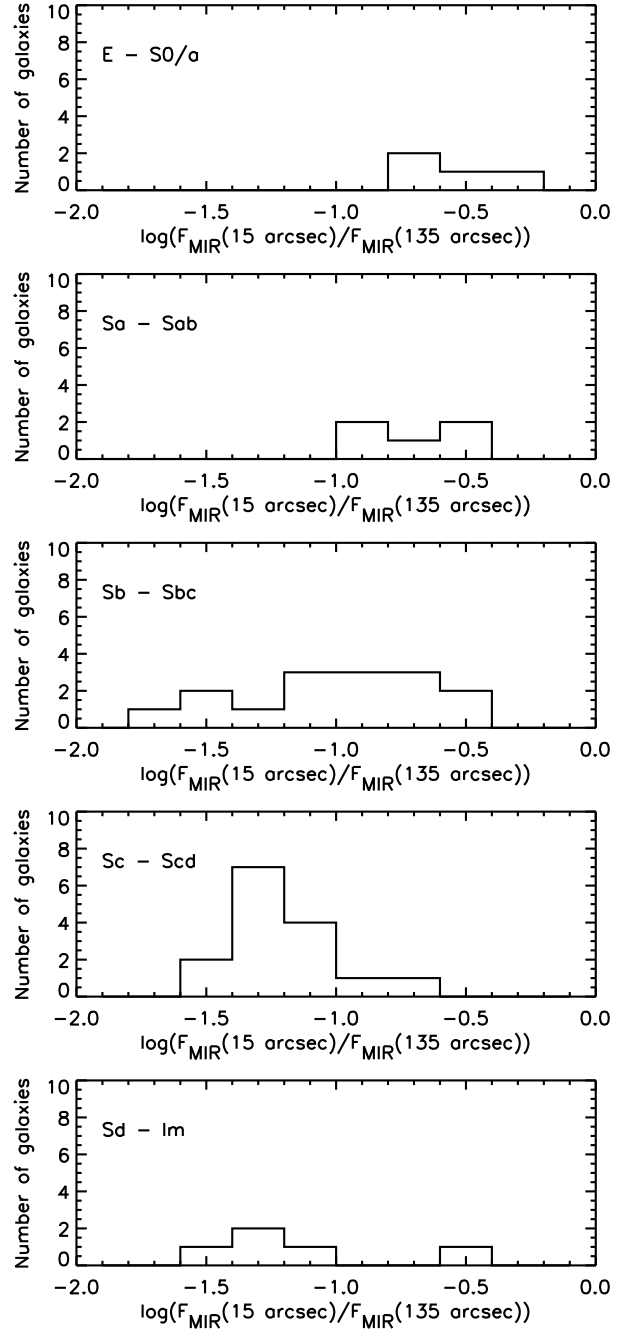


Fig. 7.— Histograms of the diagnostic of the central concentration of star formation, $\log(\frac{F_{MIR}(15'')}{F_{MIR}(135'')})$, for subsets of the galaxies in the sample binned according to Hubble type. Only galaxies where $1.5 < \log(D_{25}) < 1.9$ were used in these histograms. The diagnostic is high for galaxies that are centrally concentrated and low for galaxies that are extended.

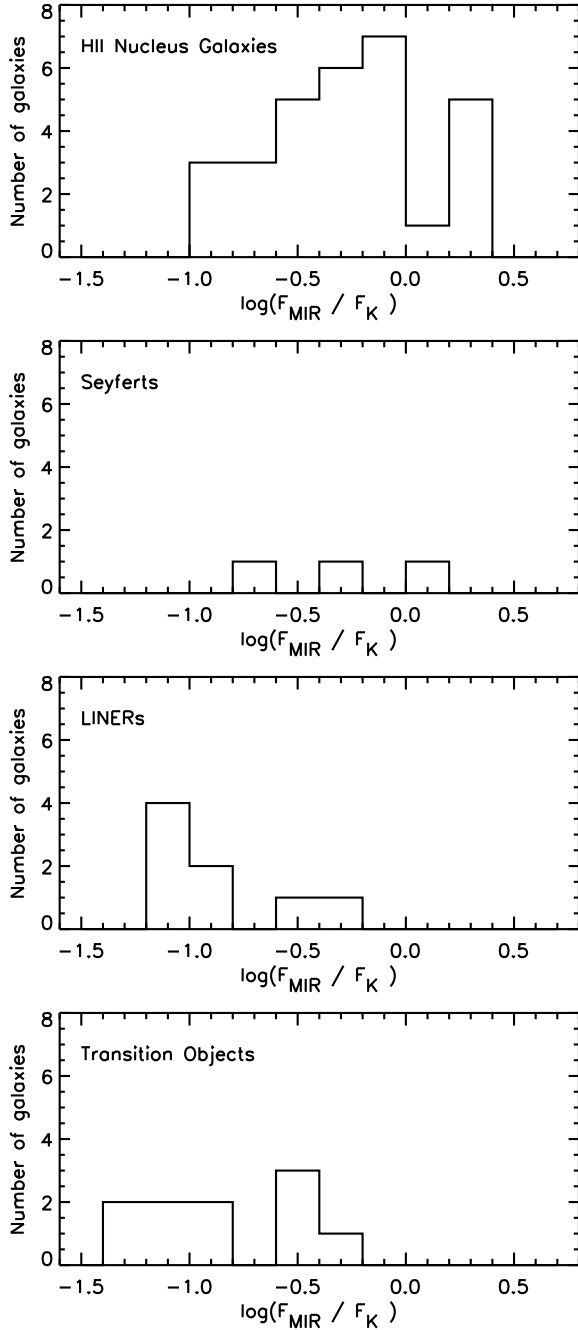


Fig. 8.— Histograms of the nuclear star formation diagnostic $\log(\frac{F_{\text{MIR}}}{F_K})$ for subsets of the galaxies in the sample based on the nuclear activity classifications in Ho, Filippenko, & Sargent (1997b). Note the relatively lower star formation activity in LINERs and transition objects compared to H II galaxies and Seyferts.

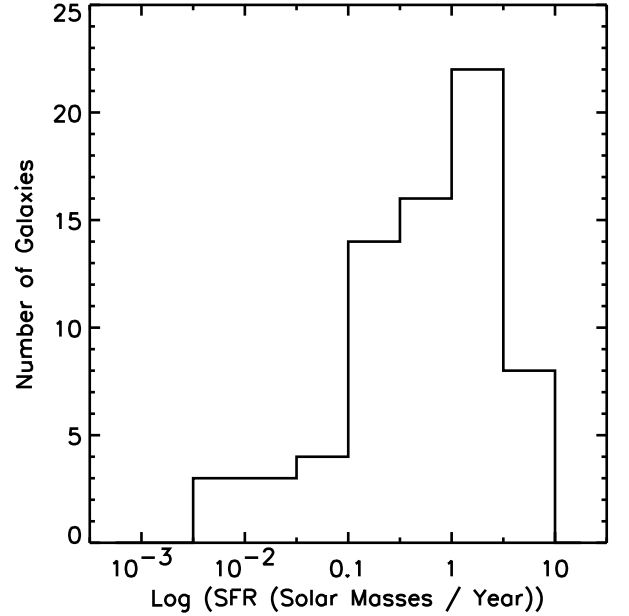


Fig. 9.— Histogram of the distribution of star formation rates for all galaxies in the sample where far-infrared luminosities were calculated.

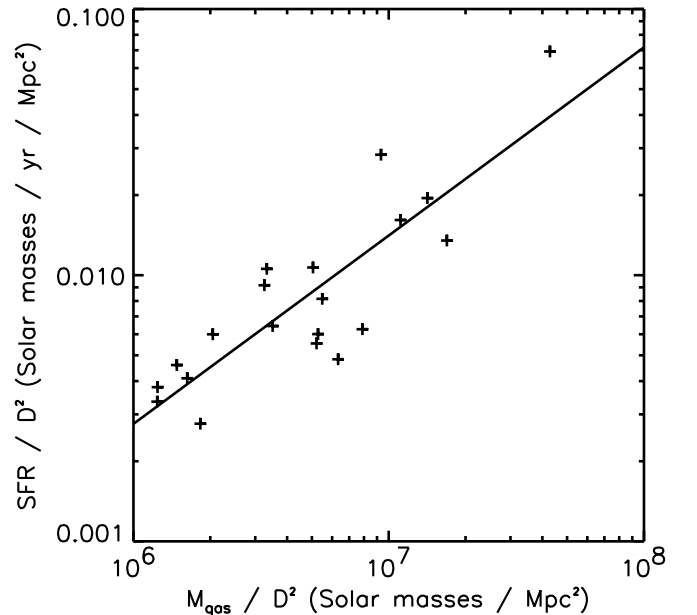


Fig. 10.— Plot of the global star formation rate versus molecular gas mass for galaxies in both the ISO and FCRAO samples. Both quantities have been normalized by the distance squared for reasons explained in the text. The line shows the best fitting power law.

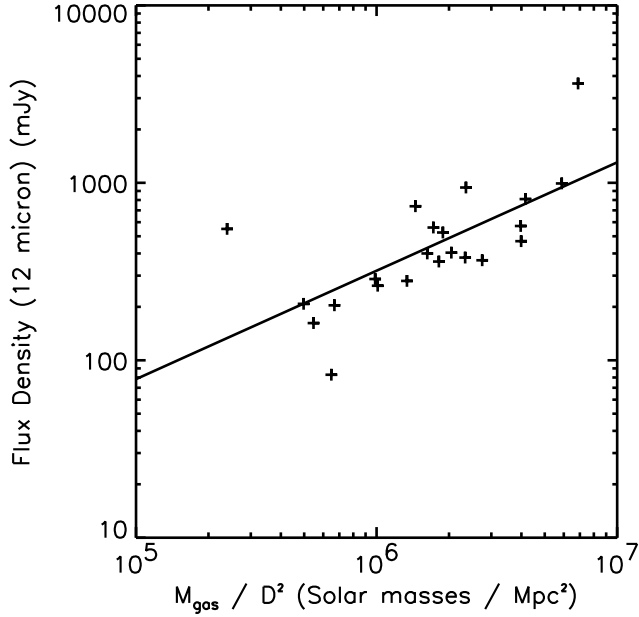


Fig. 11.— Plot of the 12 μm flux densities versus molecular gas mass for the nuclei of galaxies in both the ISO and FCRAO samples. The gas masses in this figure and Figures 12 - 14 have been normalized by the distance squared for reasons explained in the text. The lines in this figure and Figures 12 - 14 show the best fitting power laws.

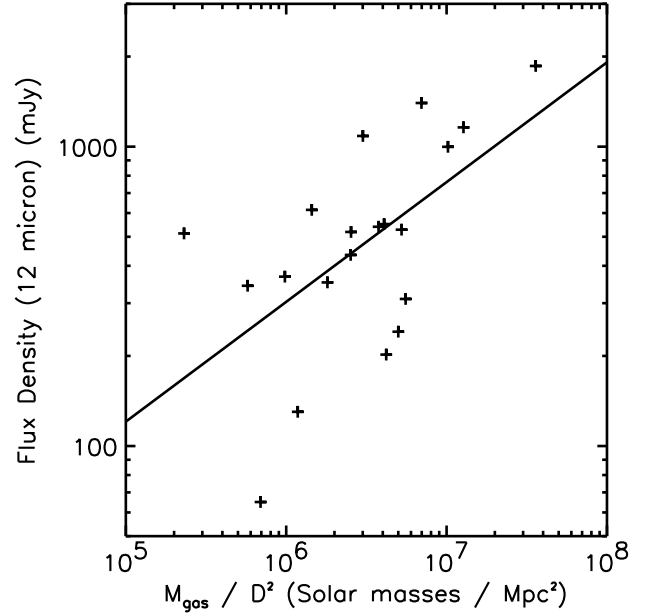


Fig. 13.— Plot of the 12 μm flux densities versus molecular gas mass for the disks of galaxies in both the ISO and FCRAO samples.

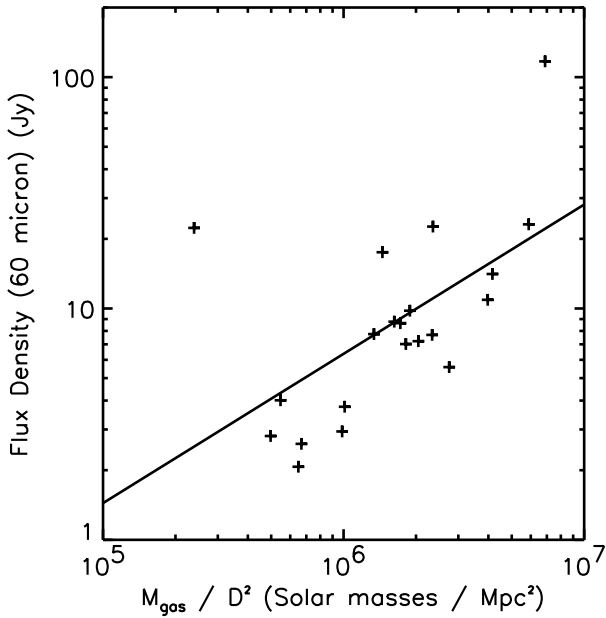


Fig. 12.— Plot of the 60 μm flux densities versus molecular gas mass for the nuclei of galaxies in both the ISO and FCRAO samples.

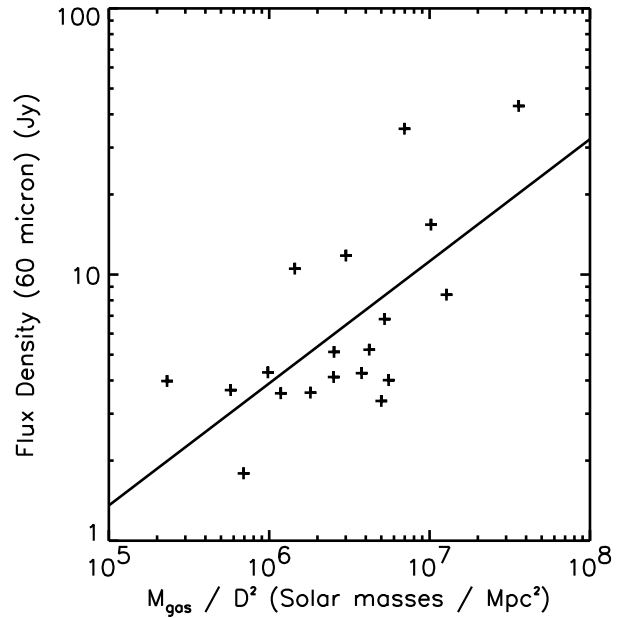


Fig. 14.— Plot of the 60 μm flux densities versus molecular gas mass for the disks of galaxies in both the ISO and FCRAO samples.

TABLE 1
RATIO OF MID- TO FAR-INFRARED FLUXES WITHIN 135'' APERTURES FOR DIFFERENT HUBBLE TYPES

Type	No. Galaxies	Mean $\log(\frac{F_{MIR}}{F_{FIR}})$
E - S0/a	6	-1.05 \pm 0.05
Sa - Sab	7	-0.94 \pm 0.02
Sb - Sbc	17	-0.94 \pm 0.03
Sc - Scd	21	-0.94 \pm 0.03
Sd - Im	6	-1.24 \pm 0.14
All	57	-0.98 \pm 0.02

TABLE 2
STAR FORMATION INDICATORS FOR DIFFERENT HUBBLE TYPES

Type	Global Star Formation		Nuclear Star Formation		Disk Star Formation	
	No. Galaxies	Mean $\log(\frac{F_{FIR}}{F_K})$	No. Galaxies	Mean $\log(\frac{F_{MIR}}{F_K})$	No. Galaxies	Mean $\log(\frac{F_{MIR}}{F_K})$
E - S0/a	11	-0.03 \pm 0.10	12	-0.92 \pm 0.11	6	-0.47 \pm 0.16
Sa - Sab	7	0.21 \pm 0.09	8	-0.69 \pm 0.10	5	-0.06 \pm 0.14
Sb - Sbc	15	0.69 \pm 0.09	17	-0.33 \pm 0.13	17	0.58 \pm 0.09
Sc - Scd	23	0.67 \pm 0.05	26	-0.30 \pm 0.07	21	0.85 \pm 0.06
Sd - Im	7	0.66 \pm 0.11	7	-0.13 \pm 0.14	6	0.87 \pm 0.12
All	63	0.50 \pm 0.05	70	-0.44 \pm 0.06	55	0.54 \pm 0.07

TABLE 3
RESULTS FROM APPLYING THE K-S TEST TO STAR FORMATION INDICATORS

Data Sets Used	Probability ^a		
	Global $\log(\frac{F_{FLR}}{F_K})$	Nuclear $\log(\frac{F_{MLR}}{F_K})$	Disk $\log(\frac{F_{MLR}}{F_K})$
Sa - Sab and Sb - Sbc	0.027	0.063	0.034
Sa - Sab and Sc - Scd	0.0010	0.021	0.0014
Sb - Sbc and Sc - Scd	0.33	0.52	0.083

^aThe probability of two data sets coming from the same distribution, as determined by applying the K-S test.

TABLE 4
MID-INFRARED SPATIAL EXTENT INDICATORS FOR DIFFERENT HUBBLE TYPES

Type	No. Galaxies	Mean $\log(\frac{F_{MIR(15'')}}{F_{MIR(135'')}})$
E - S0/a	4	-0.49 ± 0.08
Sa - Sab	5	-0.69 ± 0.07
Sb - Sbc	15	-0.99 ± 0.10
Sc - Scd	15	-1.21 ± 0.06
Sd - Im	5	-1.11 ± 0.14
All	44	-1.00 ± 0.05

TABLE 5
RESULTS FROM APPLYING THE K-S TEST TO MID-INFRARED SPATIAL EXTENT INDICATORS

Data Sets Used	Probability ^a
Sa - Sab and Sb - Sbc	0.23
Sa - Sab and Sc - Scd	0.011
Sb - Sbc and Sc - Scd	0.095

^aThe probability of two data sets coming from the same distribution, as determined by applying the K-S test.

TABLE 6
MID-INFRARED NUCLEAR STAR FORMATION INDICATORS FOR SA, SAB, AND SB GALAXIES

Type	No. Galaxies	Mean $\log(\frac{F_{MLB}}{F_K})$
SAA - SAab	2	-0.81 ± 0.38
SABa - SABab	1	-0.77
SBa - SBab	5	-0.63 ± 0.12
SAb - SAbc	6	-0.18 ± 0.19
SABb - SABbc	7	-0.46 ± 0.24
SBb - SBbc	4	-0.31 ± 0.28
SAC - SACd	11	-0.47 ± 0.09
SABc - SABcd	9	-0.25 ± 0.12
SBc - SBcd	6	-0.08 ± 0.14

TABLE 7

RESULTS FROM APPLYING THE K-S TEST TO MID-INFRARED NUCLEAR STAR FORMATION INDICATORS FOR SA AND SB GALAXIES

Data Sets Used	Probability ^a
SAa - SAab and SBa - SBab	0.96
SAb - SAbc and SBb - SBbc	0.98
SAc - SAcD and SBc - SBcd	0.16

^aThe probability of two data sets coming from the same distribution, as determined by applying the K-S test.

TABLE 8

MID-INFRARED NUCLEAR STAR FORMATION INDICATORS FOR GALAXIES WITH DIFFERENT NUCLEAR ACTIVITY TYPES

Type	No. Galaxies	Mean $\log(\frac{F_{MIR}}{F_K})$
H II Galaxies	30	-0.26 ± 0.06
Seyfert	3	-0.34 ± 0.25
LINER	8	-0.88 ± 0.11
Transition Objects	10	-0.83 ± 0.12

TABLE 9

RESULTS FROM THE K-S TEST TO MID-INFRARED NUCLEAR STAR FORMATION INDICATORS FOR GALAXIES WITH DIFFERENT NUCLEAR ACTIVITY TYPES

Data Sets Used	Probability ^a
H II Galaxies and Seyferts	0.999
H II Galaxies and LINERs	0.0023
H II Galaxies and Transition Objects	0.013
Seyferts and LINERs	0.21
LINERs and Transition Objects	0.71

^aThe probability of two data sets coming from the same distribution, as determined by applying the K-S test.